Published in "Angewandte Chemie International Edition doi: 10.1002/anie.202005069, 2020" which should be cited to refer to this work.

A Three-Dimensional Porous Organic Semiconductor Based on Fully sp^2-Hybridized Graphitic Polymer

Yearin Byun, Lilia S. Xie, Patrick Fritz, Timur Ashirov, Mircea Dincă, and Ali Coskun**

Abstract: *Dimensionality plays an important role in the charge transport properties of organic semiconductors. Although three-dimensional semiconductors, such as Si, are common in inorganic materials, imparting electrical conductivity to covalent three-dimensional organic polymers is challenging. Now, the synthesis of a three-dimensional π-conjugated porous organic polymer (3D p-POP) using catalyst-free Diels–Alder cycloaddition polymerization followed by acid-promoted aromatization is presented. With a surface area of 801 $m^2 g^{-1}$, full conjugation throughout the carbon backbone, and an electrical conductivity of $6(2) \times 10^{-4}$ $S cm^{-1}$ upon treatment with I_2 vapor, the 3D p-POP is the first member of a new class of permanently porous 3D organic semiconductors.*

Porous organic polymers (POPs) have attracted considerable attention in recent years owing to their permanent porosity, tunable pore sizes, structural modularity, large surface areas, and high physicochemical stability. In particular, POPs[1] with extended π-electron conjugation are attractive for their desirable properties in high electron mobility and electrical conductivities, allowing for low-cost and lightweight organic semiconductor applications such as light-emitting diodes, solar cells, field-effect transistors, organic lasers, battery electrodes, and photocatalysis.[2] To date, there have been a number of two-dimensional (2D) π-conjugated POPs such as thiophene-based CMP for solar cell applications[3] and I_2-doped JUC-Z2[4] for electrochemical ion sensing, as well as a growing interest in 2D porous organic semiconductors for photocatalytic water splitting.[5] Increasing the dimensionality of charge transport by creating 3D polymers with similar conductivity but higher surface areas and lower density, potentially beneficial for a number of applications such as catalysis and gas sensing, is rather challenging.[6] Indeed, the backbone of 3D POPs typically incorporates sp^3 carbon centers,[7] which break the π-conjugation and interrupt the electron delocalization along the polymer backbone.[8] Therefore, retaining full conjugation throughout the 3D backbone must exclude sp^3 carbons.

Inspiration towards this goal came from the 1946 synthesis of cubic graphite from tetraphenylene.[9] Owing to its anti-aromatic nature, the cyclooctatetraene core of tetraphenylene adopts an inherently nonplanar tub-shaped geometry, thus offering an ideal geometry to realize conjugation in 3D networks.[10] Moreover, the eight-membered cyclooctatetraene ring creates a negative Gaussian curvature,[11] which should result in high porosity as well as high electronic mobility[12] within a 3D solid. The challenge in using this building block for the construction of continuous networks is to find sufficiently mild synthetic conditions that minimize structural defects.

To this end, we recently reported[13] the synthesis of a 3D epoxy-functionalized porous organic polymer (3D ep-POP) (Figure 1). Studies[14] have revealed that the Diels–Alder reaction between furan and 1,4-epoxynaphthalene derivatives is highly stereoselective and kinetically favors the *syn-exo* product with two epoxy moieties in staggered conformation. This diastereoselectivity is conserved when cyclooctatetrafuran (**1**) and the *anti*-bisdienophile (**2**) react in dry DMF at 160 °C for 3 days to yield a 3D polymer rather than macrocycles. We surmised that the 3D ep-POP may be aromatized by acid-promoted cyclodeoxygenation, as previously reported[15] for the dehydration of oxanorbornene derivatives: a mixture of methanesulfonic acid (MsOH) and acetic anhydride (Ac_2O) produces acetyl methanesulfonate, which

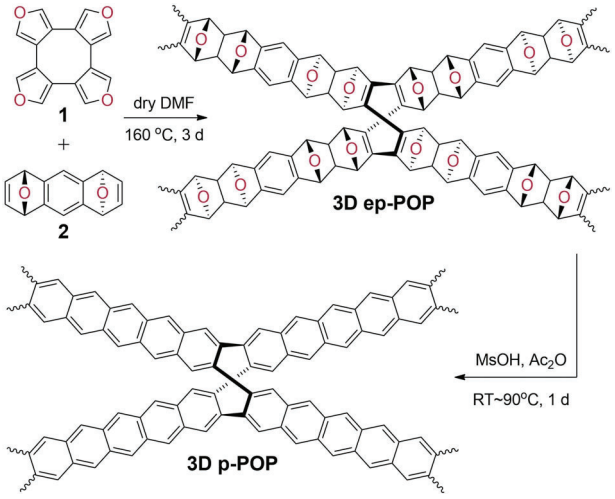

Figure 1. Synthesis of 3D ep-POP via Diels–Alder cycloaddition polymerization of **1** and **2** followed by methanesulfonic acid promoted and acetic anhydride-promoted cyclodeoxygenation to form 3D p-POP.

[*] Dr. Y. Byun
Department of Materials Science and Engineering
Korea Advanced Institute of Science and Technology (KAIST)
Daejeon 34141 (Republic of Korea)
L. S. Xie, Prof. M. Dincă
Department of Chemistry, Massachusetts Institute of Technology
77 Massachusetts Ave, Cambridge, MA 02139 (USA)
E-mail: mdinca@mit.edu
P. Fritz, T. Ashirov, Prof. A. Coskun
Department of Chemistry, University of Fribourg
Chemin de Musee 9, 1700 Fribourg (Switzerland)
E-mail: ali.coskun@unifr.ch

selectively reacts with ether groups at room temperature and promotes aromatization at elevated temperature. Treatment of the 3D ep-POP with MsOH and Ac_2O at room temperature produced an immediate color change to dark red. Heating this reaction mixture at 90 °C for 1 day under stirring, followed by thorough washing with dioxane, water, THF, and acetone, and finally Soxhlet extraction in THF for 6 days, yields a black powder.

Under acid-promoted dehydration conditions, Diels–Alder polymer adducts can be subject to three major pathways:[14b,15] 1) depolymerization via the retro-Diels–Alder reaction to furan and epoxy derivatives, 2) ring cleavage into phthalaldehyde, and 3) aromatization via cyclodeoxygenation reaction. To investigate whether the desired aromatization pathway was present here, we performed solid-state (SS) cross-polarization magic-angle spinning (CP-MAS) ^{13}C NMR spectroscopy (Figure 2a). The SS CP-MAS ^{13}C NMR spectrum of the 3D ep-POP shows multiple carbon peaks at 147, 115, 84, and 52 ppm, corresponding to both aromatic carbons and ether bridge-head carbons. In contrast, the black powder isolated after acid treatment exhibits a single peak at 131 ppm, characteristic of sp^2 carbon atoms. This result rules out pathways (1) and (2), the products of which should exhibit SSNMR peaks from aldehyde, furan, and epoxy moieties at approximately 192, 143, and 50 ppm, respectively. Thus, the majority product is the aromatization product 3D p-POP (Figure 1).

X-ray photoelectron spectroscopy (XPS) further confirmed this assignment and highlighted the changes in the electronic structure of the C atoms upon aromatization (Figure 2b; Supporting Information, Figure S1). The bond energies, corresponding to chemical bonds and percentages of atomic concentration, are summarized in the Supporting Information, Tables S1 and S2. Notably, before the aromatization reaction, the presence of epoxy groups was confirmed with C 1s peaks at 284.5, 286.4, and 288.6 eV. Also, the O 1s spectrum (Supporting Information, Figure S1) showed strong speaks at 46.4 and 53.6 eV for C–O and C–O–C, respectively. After aromatization, the strong C 1s peak at 285.6 eV assigned to the sp^3 C–C bonds disappears, whereas the peak corresponding to sp^2 C–C bonds persists at 284.5 eV.

Vibrational spectroscopy corroborates the SS NMR and XPS data. The Fourier-transform infrared spectroscopy (FTIR) spectrum of the 3D ep-POP (Figure 2c) exhibits a band at 1110 cm^{-1} for the ether C–O–C stretching band, which disappears upon aromatization. Aromatization also gives rise to in-plane and out of plane C–H bending modes at 1080–1035 cm^{-1} and at 907–731 cm^{-1}, respectively, which are in good agreement with the FTIR spectrum of pentacene.[16] Finally, the stretching bands at 1661, 1603 cm^{-1}, and 1453 cm^{-1} are assigned to the in-ring C–C stretching vibrations, which only appear after aromatization and are not present for the 3D ep-POP. A Raman spectrum of the 3D p-POP (Figure 2d) obtained under excitation at 325 nm exhibits two strong peaks at 1387 and 1589 cm^{-1}. These can be attributed to C–C ring stretching vibration, A_g mode, and in plane vibrational mode, B_{3g}, respectively, and match well the Raman bands[17] of pentacene, further confirming that the 3D p-POP has molecular connectivity based on pentacene moieties. Generally, linear polyacene molecules such as pentacene are known to be kinetically unstable under ambient atmospheric conditions in the presence of light and air, in which the molecule undergoes photooxidation. However, the pentacene units

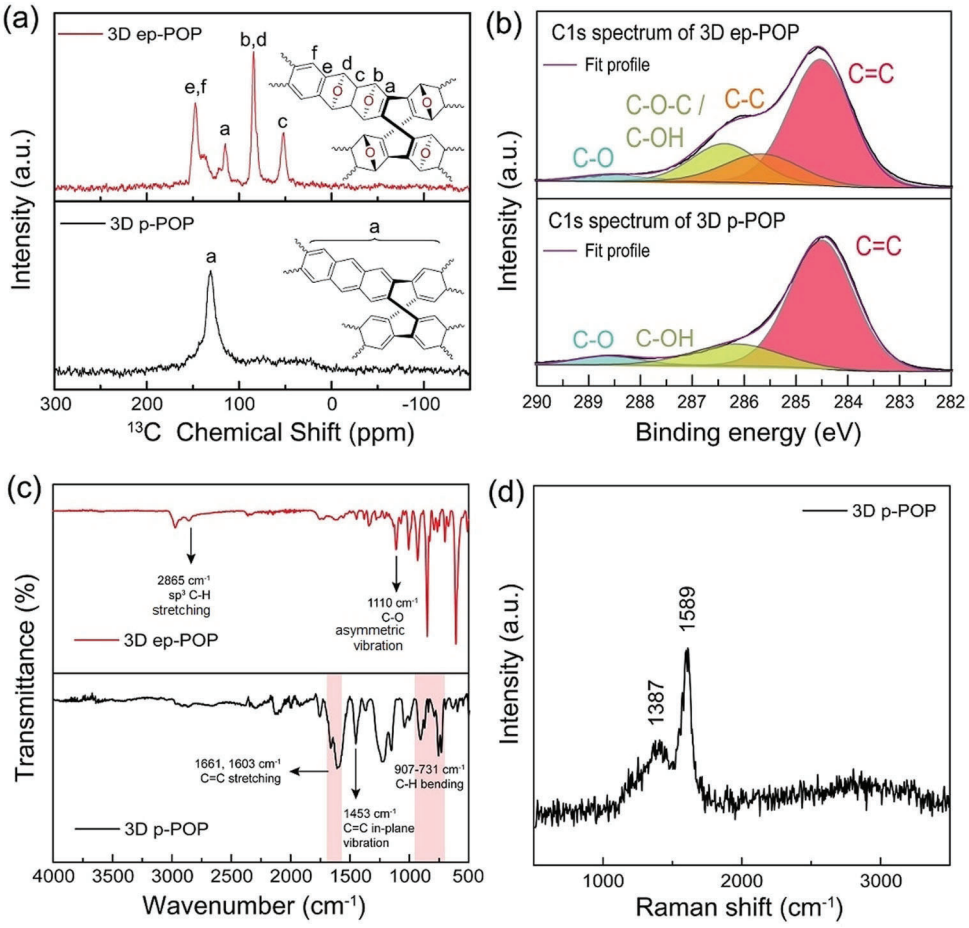

Figure 2. Spectroscopic characterizations of 3D ep-POP and 3D p-POP a) Solid-state CP-MAS ^{13}C NMR spectra of 3D ep-POP and p-POP. b) C 1s XPS spectra of 3D POPs. c) FTIR spectra of 3D POPs d) Raman spectra of 3D p-POP measured at 325 nm (3.81 eV) on powder samples.

were successfully stabilized in the polymer network, wherein the fused cyclooctatetraene rings minimize the rate of decomposition.[18]

Expectedly, powder X-ray diffraction (PXRD) analysis (Supporting Information, Figure S2) of 3D ep-POP and 3D p-POP showed broad features at $2\theta = 18°$ and 22°, respectively, which indicate that the polymeric networks are mostly amorphous. Morphologically, both 3D ep-POP and 3D p-POP appear as spherical particles with an average diameter of 1 μm, as determined by field-emission scanning electron microscopy (FE-SEM; Supporting Information, Figure S3).

Comparative thermogravimetric analysis (TGA) of 3D ep-POP and 3D p-POP further supported the formation of 3D p-POP (Supporting Information, Figure S4). Aside from the higher moisture content of 3D ep-POP, which is expected considering its higher oxygen content, a subsequent mass loss at 250 °C assigned to the extrusion of the ether bridges in the 3D ep-POP. Notably, the 3D p-POP does not exhibit the mass loss event at 250 °C, pointing to the lack of dehydratable cyclic ether units and thus complete aromatization.

To study the porosity and textural properties of 3D ep-POP and 3D p-POP, we measured Ar adsorption isotherms at 87 K. Both materials exhibit Type I isotherms (Figure 3). Significant adsorption at low partial pressures and also the observed broad hysteresis in the entire pressure range for the desorption branch were attributed to the microporosity and swelling of the framework, respectively. Fitting these to the Brunauer–Emmett–Teller (BET) equation in the pressure range $P/P_0 < 0.1$ (Supporting Information, Figure S5) gave specific surface area and micropore surface area of 779 and 462 $m^2 g^{-1}$, respectively, for the 3D ep-POP. After aromatization, the specific surface area as well as micropore surface area increase to 801 and 501 $m^2 g^{-1}$, respectively, for the 3D p-POP. The augmented surface area is likely the result of the increased rigidity of the polymer backbone upon aromatization. The presence of interpenetrated polymer network structure as verified by the PXRD data pointing to the π–π stacking interactions between the pentacene linkers is likely to limit a further increase in the surface area. Nevertheless, the permanent porosity of the 3D p-POP exceeds that of carbon allotropes such as C_{60}[19] (0.3 $m^2 g^{-1}$), and graphene[20] (300 $m^2 g^{-1}$) and is comparable to carbon based 3D POPs such as GNF-1[7] (679 $m^2 g^{-1}$). We utilized nonlocal density functional theory (NLDFT) based on the carbon-slit pores model to obtain the pore size distribution plots (Figure 3), which showed that both polymers contain ultramicropores of 0.4 and 0.41 nm for 3D ep-POP and 3D p-POP, respectively.

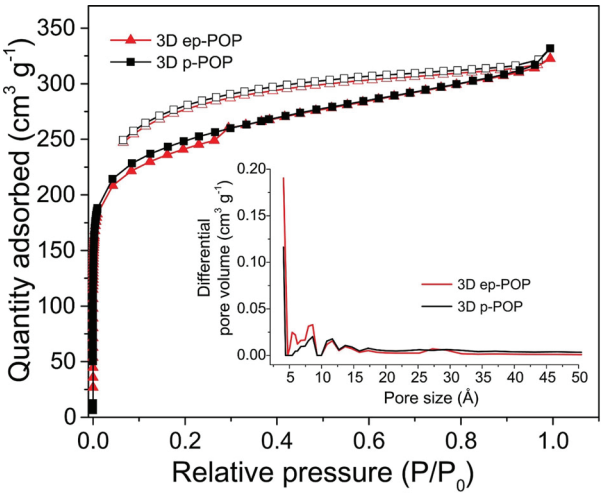

Figure 3. Argon adsorption–desorption isotherms of 3D ep-POP and p-POP at 87 K. Filled and empty symbols represent gas adsorption and desorption, respectively. Inset: NLDFT pore-size distributions of 3D POPs.

Two-probe measurements of pressed pellets[21] of 3D p-POP yielded a conductivity of $5(3) \times 10^{-8}$ S cm^{-1} (Table 1) at room temperature (296 K). This value is nearly two orders of magnitude higher than the conductivity of the unaromatized precursor, 3D ep-POP ($8(1) \times 10^{-10}$ S cm^{-1}). This is consistent with a greater degree of charge delocalization in the conjugated 3D p-POP, but is likely diminished by the lack of charge carriers in the material.[22] To increase the latter, samples of 3D p-POP were exposed to I_2 vapor (0.03 torr) for 16 h at 296 K. According to the TGA data, the iodine uptake under these conditions is approximately 25 wt % (Supporting Information, Figure S7). Iodine incorporation into I_2@3D p-POP was confirmed by XPS (Supporting Information, Figure S8), which revealed iodine peaks at 630 and 619.8 eV, corresponding to the $3d_{3/2}$ and $3d_{5/2}$ transitions of iodine, respectively. Notably, doping of 3D p-POP with I_2 increases the conductivity by four orders of magnitude relative to the native 3D p-POP, reaching an average value of $6(2) \times 10^{-4}$ S cm^{-1} (For the comparison of conductivities with previously reported POPs and COFs, see the Supporting Information, Table S4). Comparison of the diffuse reflectance UV/Vis-NIR and diffuse reflectance infrared Fourier transform spectroscopy (DRIFTS) spectra of 3D p-POP and I_2@3D p-POP revealed a red-shifted absorption onset for the latter (Figure 4a) and a decrease in the optical band gap from 0.65 eV to 0.47 eV (Supporting Information, Figure S9). After exposure to vacuum for 8 h, the conductivity decreased slightly to $2.9(3) \times 10^{-5}$ S cm^{-1}, indicating that the doping was only partially reversible under vacuum, and that the increased conductivity is robust in I_2@3D p-POP.

Variable-temperature conductance measurements (Supporting Information, Figure S9) of 3D p-POP and I_2@3D p-POP revealed semiconducting behavior for both materials between 250 and 320 K (Figure 4b). Fitting the data to the Arrhenius equation for thermally activated transport, $G = G_0 \exp(-E_a/k_B T)$, where G is the conductance, G_0 is a prefactor, k_B is the Boltzmann constant, and T is the absolute temperature, yielded values for E_a of 0.25 eV for 3D p-POP, and 0.17 eV for I_2@3D p-POP. The smaller value of E_a for the I_2-doped material is consistent with the smaller band gap.

Table 1: Electrical conductivity values at 296 K of 3D ep-POP, 3D p-POP, I_2@p-POP, and I_2@3D p-POP after 8 h under vacuum.

Material	Conductivity [S cm^{-1}]
3D ep-POP	$8(1) \times 10^{-10}$
3D p-POP	$5(3) \times 10^{-8}$
I_2@p-POP	$6(2) \times 10^{-4}$
I_2@p-POP, 8 h vacuum	$2.9(3) \times 10^{-5}$

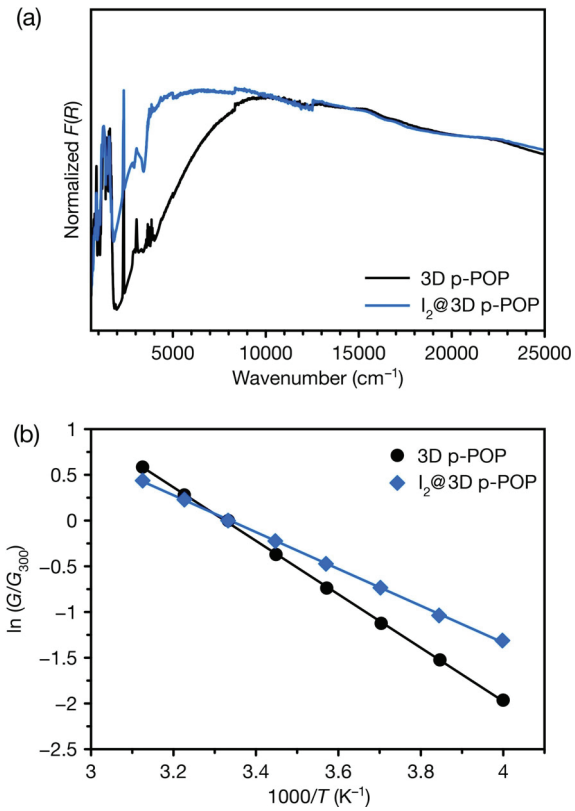

Figure 4. a) Diffuse reflectance UV/Vis-NIR and DRIFTS spectra of 3D p-POP and I_2@3D p-POP. b) Variable-temperature conductance of 3D p-POP and I_2@3D p-POP, showing thermally activated transport.

Overall, the marked enhancement of conductivity upon I_2 treatment, along with the optical and VT conductivity data, indicates that 3D p-POP is readily hole-doped. The range of conductivities accessible over six orders of magnitude from the unaromatized 3D ep-POP to the doped I_2@3D p-POP demonstrates the tunability of this class of materials. Their semiconducting properties should open new doors for applications and fundamental studies of porous, sp^2-hybridized 3D organic semiconductors.

In summary, we have introduced a new class of three-dimensional porous organic polymer integrating a π-electronic component, that is pentacene, while retaining a permanently porous structure. The resulting 3D p-POP showed semiconducting properties by maintaining electron mobility and increased stability of pentacene within the polymer network. The resulting 3D p-POP showed many desirable features, such as physicochemical stability, permanent porosity, high surface area, and semiconducting properties. This approach is expected to expand the synthetic strategy for the fields of not only 3D carbon materials but also of π-conjugated porous organic polymers, with potential utilization in organic semiconductor applications such as light-emitting diodes, solar cells, field-effect transistors, organic lasers, and photocatalysis.

Acknowledgements

A.C. thanks the Swiss National Science Foundation (SNSF) for funding of this research (200021-175947). Work in the Dincă lab (L.S.X. and M.D.) was supported by the U.S. Department of Energy, Office of Science, Office of Basic Energy Sciences (DE-SC0018235). L.S.X. thanks the National Science Foundation for support through the Graduate Research Fellowship Program (1122374).

Conflict of interest

The authors declare no conflict of interest.

Keywords: 3D carbon allotropes · Diels–Alder polymerization · microporous materials · organic semiconductors · porous organic polymers

[1] a) C. M. Thompson, F. Li, R. A. Smaldone, *Chem. Commun.* **2014**, *50*, 6171 – 6173; b) P. Arab, M. G. Rabbani, A. K. Sekizkardes, T. İslamoğlu, H. M. El-Kaderi, *Chem. Mater.* **2014**, *26*, 1385 – 1392; c) Y. Byun, S. H. Je, S. N. Talapaneni, A. Coskun, *Chem. Eur. J.* **2019**, *25*, 10262 – 10283.

[2] a) J. Byun, K. A. I. Zhang, *Mater. Horiz.* **2020**, *7*, 15 – 31; b) F. Vilela, K. Zhang, M. Antonietti, *Energy Environ. Sci.* **2012**, *5*, 7819 – 7832; c) T. Zhang, G. Xing, W. Chen, L. Chen, *Mater. Chem. Front.* **2020**, *4*, 332 – 353.

[3] C. Gu, N. Huang, Y. Chen, L. Qin, H. Xu, S. Zhang, F. Li, Y. Ma, D. Jiang, *Angew. Chem. Int. Ed.* **2015**, *54*, 13594 – 13598; *Angew. Chem.* **2015**, *127*, 13798 – 13802.

[4] T. Ben, S. Qiu, *CrystEngComm* **2013**, *15*, 17 – 26.

[5] a) R. S. Sprick, Y. Bai, A. A. Y. Guilbert, M. Zbiri, C. M. Aitchison, L. Wilbraham, Y. Yan, D. J. Woods, M. A. Zwijnenburg, A. I. Cooper, *Chem. Mater.* **2019**, *31*, 305 – 313; b) J. Lee, O. Buyukcakir, T.-w. Kwon, A. Coskun, *J. Am. Chem. Soc.* **2018**, *140*, 10937 – 10940; c) S. Kuecken, A. Acharjya, L. Zhi, M. Schwarze, R. Schomäcker, A. Thomas, *Chem. Commun.* **2017**, *53*, 5854 – 5857.

[6] a) L. S. Xie, G. Skorupskii, M. Dincă, *Chem. Rev.* **2020**, https://doi.org/10.1021/acs.chemrev.1029b00766; b) P. J. Skabara, J.-B. Arlin, Y. H. Geerts, *Adv. Mater.* **2013**, *25*, 1948 – 1954.

[7] Y. Byun, A. Coskun, *Chem. Mater.* **2015**, *27*, 2576 – 2583.

[8] a) O. K. Farha, A. M. Spokoyny, B. G. Hauser, Y. S. Bae, S. E. Brown, R. Q. Snurr, C. A. Mirkin, J. T. Hupp, *Chem. Mater.* **2009**, *21*, 3033 – 3035; b) S. H. Je, O. Buyukcakir, D. Kim, A. Coskun, *Chem* **2016**, *1*, 482 – 493; c) O. Buyukcakir, S. H. Je, D. S. Choi, S. N. Talapaneni, Y. Seo, Y. Jung, K. Polychronopoulou, A. Coskun, *Chem. Commun.* **2016**, *52*, 934 – 937; d) J. Roncali, P. Leriche, A. Cravino, *Adv. Mater.* **2007**, *19*, 2045 – 2060.

[9] J. Gibson, M. Holohan, H. L. Riley, *J. Chem. Soc.* **1946**, 456 – 461.

[10] S. N. Talapaneni, J. Kim, S. H. Je, O. Buyukcakir, J. Oh, A. Coskun, *J. Mater. Chem. A* **2017**, *5*, 12080 – 12085.

[11] T. Fallon, A. C. Willis, A. D. Rae, M. N. Paddon-Row, M. S. Sherburn, *Chem. Sci.* **2012**, *3*, 2133 – 2137.

[12] S. Hahn, S. Koser, M. Hodecker, P. Seete, F. Rominger, O. Š. Miljanić, A. Dreuw, U. H. F. Bunz, *Chem. Eur. J.* **2018**, *24*, 6968 – 6974.

[13] Y. Byun, A. Coskun, *Angew. Chem. Int. Ed.* **2018**, *57*, 3173 – 3177; *Angew. Chem.* **2018**, *130*, 3227 – 3231.

[14] a) P. R. Ashton, G. R. Brown, N. S. Isaacs, D. Giuffrida, F. H. Kohnke, J. P. Mathias, A. M. Z. Slawin, D. R. Smith, J. F. Stoddart, D. J. Williams, *J. Am. Chem. Soc.* **1992**, *114*, 6330 –

6353; b) S. Eda, F. Eguchi, H. Haneda, T. Hamura, *Chem. Commun.* **2015**, *51*, 5963 – 5966.
[15] E. Mahmoud, J. Yu, R. J. Gorte, R. F. Lobo, *ACS Catal.* **2015**, *5*, 6946 – 6955.
[16] K. P. Weidkamp, A. Afzali, R. M. Tromp, R. J. Hamers, *J. Am. Chem. Soc.* **2004**, *126*, 12740 – 12741.
[17] S. Wood, G.-P. Rigas, A. Zoladek-Lemanczyk, J. C. Blakesley, S. Georgakopoulos, M. Mas-Torrent, M. Shkunov, F. A. Castro, *Sci. Rep.* **2016**, *6*, 33057.
[18] S. R. Bheemireddy, P. C. Ubaldo, P. W. Rose, A. D. Finke, J. Zhuang, L. Wang, K. N. Plunkett, *Angew. Chem. Int. Ed.* **2015**, *54*, 15762 – 15766; *Angew. Chem.* **2015**, *127*, 15988 – 15992.
[19] A. Martínez-Alonso, J. M. D. Tascón, E. J. Bottani, *Langmuir* **2000**, *16*, 1343 – 1348.
[20] Z. W. Zhu, Q. R. Zheng, *Appl. Therm. Eng.* **2016**, *108*, 605 – 613.
[21] L. Sun, S. S. Park, D. Sheberla, M. Dincă, *J. Am. Chem. Soc.* **2016**, *138*, 14772 – 14782.
[22] a) C. K. Chiang, Y. W. Park, A. J. Heeger, H. Shirakawa, E. J. Louis, A. G. MacDiarmid, *J. Chem. Phys.* **1978**, *69*, 5098 – 5104; b) X. Guan, F. Chen, Q. Fang, S. Qiu, *Chem. Soc. Rev.* **2020**, *49*, 1357 – 1384.

Manuscript received: April 7, 2020
Revised manuscript received: May 2, 2020
Accepted manuscript online: May 12, 2020
Version of record online: ■■ ■■, ■■■■

Communications

Organic Semiconductors

Y. Byun, L. S. Xie, P. Fritz, T. Ashirov, M. Dincă,* A. Coskun* ____ ▮▮▮▮–▮▮▮▮

A Three-Dimensional Porous Organic Semiconductor Based on Fully sp^2-Hybridized Graphitic Polymer

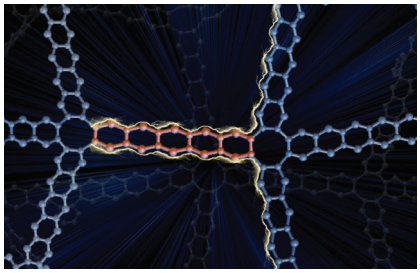

3D p-POP! A 3D π-conjugated porous organic polymer incorporating in situ formed pentacene linkers was synthesized through a catalyst-free Diels–Alder cycloaddition polymerization and an acid-promoted aromatization reaction. The resulting polymer shows high electrical conductivity and is the first member of a class of permanently porous 3D organic semiconductors.